

A Computational Model for Motor Pattern Switching Between Taste-induced Ingestion
and Rejection Oromotor Behaviors

Sharmila Venugopal¹, Joseph B Travers² and David H Terman³

¹ Neuroscience Graduate Studies Program, ² Department of Oral Biology, ³ Department
of Mathematics and Mathematical Biosciences Institute
The Ohio State University

Running head: Motor Pattern Switching

34 Pages

9 Figures

1 Table

Correspondence:

Sharmila Venugopal

Mailing Address: 305 W 12th Avenue, Columbus, OH-43210

Email: venugopal.7@osu.edu

Phone: 614-292-4046

Fax: 614-247-6945

Keywords: central pattern generator, brainstem, bursting oscillations

Abstract

The mechanism of switching activity patterns in a central pattern generator is fundamental to the generation of diverse motor behaviors. Based on what is known about a brainstem substrate mediating the oral components of ingestion and rejection, we use computational techniques to construct a hypothetical multifunctional network that switches between the motor outputs of ingestion (licking) and rejection (gaping). The network is constructed using single-compartment conductance-based models for individual neurons based on Hodgkin-Huxley formalism. Using a fast-slow reduction and geometric analysis we describe a mechanism for pattern switching between licks and gapes. The model supports the hypothesis that a single configuration of network connections can produce both activity patterns. It further predicts that prolonged inhibition of some network neurons could lead to a switch in network activity from licks to gapes.

1 Introduction

Switching between activity patterns in a central pattern generator (CPG) is fundamental to the generation of diverse motor behaviors. Such switching is often initiated by a specific sensory input (Kupfermann, 1974; Marder & Pearson, 1998). In the taste system for example, palatable substances such as sucrose or sodium chloride initiate ororhythmic ingestive licking responses. Bitter (often toxic) substances such as quinine monohydrochloride, also initiate ororhythmic activity, but in contrast to licking, this ororhythmic activity serves to expel fluid from the mouth. These oral rejection responses are called "gapes" and have been characterized in both rodent and primate (including human) species (Grill & Norgren, 1978; Steiner, 1973). These ororhythmic responses of ingestion and rejection are organized in the lower brainstem which contains sensory, premotor and motor neurons necessary for these behaviors (Travers *et al.*, 1997; Grill & Kaplan, 2002).

Licking and gaping can be characterized electromyographically (EMG) from a subset of orolingual muscles including the anterior digastric (AD: jaw-opener); genioglossus (GEN: lingual protruder) and styloglossus, (STY: lingual retractor) muscles (Travers & Norgren, 1986; Dinardo & Travers, 1994). The lick EMG pattern differs from the gape EMG pattern in terms of rate, amplitude, duration and phase sequence of muscle activity. Lick cycles are characterized by a stereotypical alternating two-phase sequence of coincident GEN and AD activity (Phase I), followed by STY activity (Phase II). Gape cycles are characterized by a three-phase sequence with an initial co-activation of the AD and STY muscles (Phase I), followed by coincident peaking of AD and GEN activity (Phase II) and terminating with an additional burst of activity in STY (Phase III). Lick cycles repeat at about 7 Hz while gape cycles repeat at about 3-4 Hz. In addition to the phase changes between lingual and masticatory muscle activity that differentiates a lick from a gape, gapes also show larger amplitude and longer duration EMG AD activity, consistent with the behavioral characterization of an oral "gape".

Several lines of evidence suggest that licks and gapes are organized by a common neural network (reviewed in (Travers *et al.*, 1997)). At the single cell level, chronic unit recording studies in the medullary reticular formation (RF), an area rich in pre-oromotor neurons, indicated that a large proportion of neurons active during licking were also active during gaping (Travers *et al.*, 2000). Further indicative of a common neural substrate, licks and gapes were equally suppressed by reversible lesions induced by local RF infusions of the GABA_A agonist, muscimol (Chen *et al.*, 2001). Similarly, infusions of glutamate antagonists into the same RF region equally suppressed both behaviors (Chen & Travers, 2003), suggesting that activation of glutamate receptors is a necessary condition to their expression. In contrast, infusions of inhibitory amino acid antagonists enhanced the amplitude of EMG activity associated with both behaviors suggesting, perhaps, a level of tonic inhibition within the network (Chen & Travers, 2003). These results suggest that disinhibition could play a role in increasing the amplitude of motor responses that are associated with gapes. However, even if true, disinhibition does not lead to a simple explanation of how the phase switching associated with the transition from licks to gapes is accomplished.

Thus, the goal of the present study is to construct a biophysical model for the lick-gape CPG network to gain insight into the underlying mechanism of phase switching associated with the transition from licks to gapes. We show that a minimal biophysical model with three classes of premotor interneurons is capable of generating activity patterns similar to licks and gapes. We also present a geometric analysis of the two patterns of neural responses using a fast-slow reduction of the system of equations. Our analysis leads to conditions that may be responsible for the change in neural firing patterns in a CPG network, resulting in the different motor behaviors of ingestion and rejection.

2 Methods

2.1 Background

The lick-gape biophysical model we have developed was derived from the connectional model of brainstem sensory-motor pathways shown in Figure 1. The general schema of connectivity between sensory, interneuronal and motor neurons is reasonably well established (reviewed in (Travers *et al.*, 1997)). Sensory fibers carrying taste information from taste receptors on the tongue synapse on neurons in the nucleus of solitary tract (NST). Interneurons in the medullary RF receive excitatory input from NST and form the CPG for taste-induced licks and gapes. The CPG is composed of three classes of premotor interneurons: pre-jaw-opener (O), pre-lingual-protruder (P) and pre-lingual-retractor (R). The CPG drives AD (jaw-opener muscle) motoneurons in the motor trigeminal nucleus (mV), and GEN (lingual protruder muscle) and STY (lingual retractor muscle) motoneurons in the hypoglossal nucleus (mXII). Axons of these motor neurons innervate the corresponding muscles to generate lick and gape EMG patterns. Further, we posited a specific pattern of mutual inhibition between the 3 classes of interneurons, O, R and P (see Figure 1). Although there is some neurophysiological data to support such inhibition (Inoue *et al.*, 1994), the precise pattern illustrated has yet to be empirically validated. Mutual inhibition between the interneurons is shown as a direct inhibitory connection for computational simplicity.

The basic firing properties of the interneurons in the model were derived from indirect sources, i.e. extracellular recording. Although neurophysiological recordings from interneurons in the medullary RF during licking and gaping have revealed a variety of neuron types (Travers *et al.*, 2000), a significant proportion were classified as "lick-rhythmic" based on a tight correlation with AD activity during licking. We re-evaluated some of these data to find a reasonable basis on which to construct the biophysical model. This

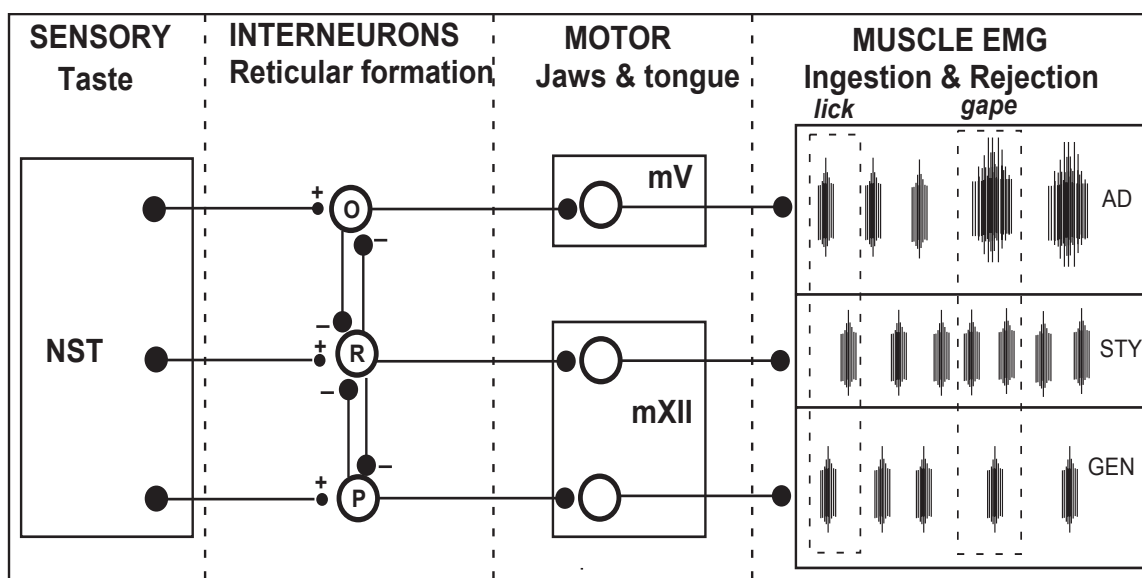
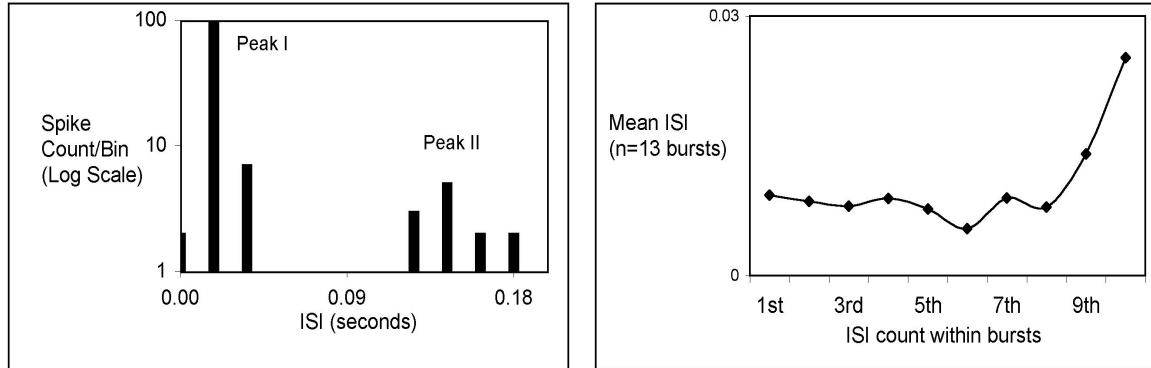


Figure 1: Sensori-Motor pathway for taste-induced licks and gapes; Projections from the first order gustatory relay, the nucleus of the solitary tract (NST) excite pre-oro-motor interneurons in the brainstem reticular formation. Mutual inhibition between interneurons (O: Pre-jaw opener neuron, R: Pre-tongue retractor neuron, P: Pre-tongue protrudor neuron) provides a mechanism for pattern switching (see text). Interneurons project to oromotor nuclei (mXII: Hypoglossal Nucleus, mV: Motor Trigeminal Nucleus) that innervate lingual and masticatory muscles involved in licks and gapes. Typical EMG pattern and the phase sequencing in a jaw-opener muscle (AD), tongue protrudor muscle (GEN) and tongue retractor muscle (STY) during licks and gapes are shown.

re-analysis of lick-rhythmic units (from (Travers *et al.*, 2000)) revealed that a majority of neurons showed a bi-modal distribution of inter-spike intervals (ISI), characteristic of cells with bursting activity (see Figure 2(a)). The ISI distribution consists of 2 peaks. Peak-I occurs at about 0.02 ms (frequency ≈ 50 Hz) corresponding to within burst spikes and peak-II at about 0.15 ms (frequency ≈ 7 Hz) corresponds to the inter-burst interval. Additionally, the distribution of ISI values within bursts was further analyzed. The distribution of serial ISI values within a burst showed a trend for increasing ISIs, indicative of a burst structure with decreasing spike frequency. For example, Figure 2(b) shows the increasing trend in mean ISI computed from a series of bursts for a single lick-rhythmic neuron. This is characteristic of square-wave bursting cells (Rinzel, 1985). Thus, as an



(a) Bimodal inter-spike interval (ISI) distribution of an identified lick-rhythmic premotor neuron in the IRT; Peak I corresponds to inter-spike intervals within bursts with spike frequency of ≈ 50 Hz, peak II corresponds to inter-burst interval with burst frequency of ≈ 7 Hz.

(b) Mean ISI trend within bursts in the same cell shows increasing ISI values (or reducing frequency of spikes) towards the end of bursts

Figure 2: Bursting unit example.

initial step in constructing the biophysical model, we attributed this square-wave bursting characteristic to the 3 classes of interneurons in the model.

2.2 Lick-Gape CPG Network Model

We consider a network of three neurons, as shown in Figure 3, representing the lick-gape CPG. Synaptic coupling between R and P cells is hypothetically modeled as reciprocal inhibition. Coupling between O and R is modeled as mutual inhibition and there is no direct coupling between O and P.

Since not much is known about the intrinsic or synaptic properties of these neurons, we have considered a minimal model of a bursting neuron for each cell in the network. Each cell is modeled as a single-compartment conductance-based biophysical model for a square-wave bursting neuron (Rinzel & Ermentrout, 1998) based on Hodgkin-Huxley formalism (Hodgkin & Huxley, 1952). The equations for each cell are:

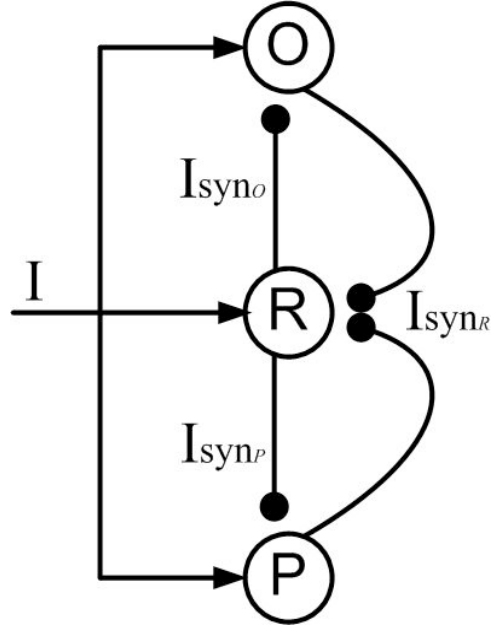


Figure 3: Lick-gape CPG network model; I represents non-rhythmic excitatory input posited to be from NST. I_{syn_O} , I_{syn_R} and I_{syn_P} represent inhibitory synaptic input to O, R and P respectively

$$C_m \frac{dV_i}{dt} = -(I_{L_i} + I_{Ca_i} + I_{K_i} + I_{KCa_i} - I + I_{syn_i}) \quad (1)$$

$$\frac{dw_i}{dt} = \phi \frac{w_\infty(V_i) - w_i}{\tau(V_i)} \quad (2)$$

$$\frac{dCa_i}{dt} = \varepsilon(-\mu I_{Ca_i} - Ca_i) \quad (3)$$

$$\frac{ds_i}{dt} = \alpha(1 - s_i)s_\infty(V_i) - \beta_i s_i \quad (4)$$

where $i = O$ or R or P .

Equation (1) describes the membrane current balance equation for each cell. Here, V_i represents the membrane potential and C_m is the membrane capacitance. In equation (1), $I_{L_i} = g_L \times (V_i - V_L)$ is the leak current, $I_{Ca_i} = g_{Ca} \times m_\infty(V_i) \times (V_i - V_{Ca})$ is an inward calcium current, $I_{K_i} = g_K \times w_i \times (V_i - V_K)$ is an outward potassium current, $I_{KCa_i} = g_{KCa} \times z_i \times (V_i - V_K)$ is an intracellular Ca^{2+} -activated outward K^+ current, and I represents excitatory drive

to the network posited to be mainly from the NST. The constants g_L , g_{Ca} , g_K and g_{KCa} represent maximal conductances and V_L , V_{Ca} and V_K represent reversal potentials for I_L , I_{Ca} , I_K and I_{KCa} , respectively. Note that w_i is the channel gating variable for I_{K_i} . Moreover, z_i is a Ca^{2+} dependent gating variable for I_{KCa_i} with a Hill-like dependence on the near-membrane Ca^{2+} concentration, and is defined as $z_i = \frac{Ca_i}{1+Ca_i}$. In equation (2), $w_\infty(V_i)$ is the steady-state K^+ activation and $\tau_\infty(V_i)$ is the voltage-dependent time constant for K^+ channels; ϕ is a temperature-like time scale factor. Equation (3) describes the calcium dynamics. The parameter μ is for converting current into a concentration flux and involves the ratio of the cell's surface area to the calcium compartment's volume. The parameter ε is a product of the calcium removal rate and the ratio of free to total calcium in the cell. Since calcium is highly buffered, ε is small and thus the calcium dynamics are slow. In equation (1), I_{syn_i} represents synaptic coupling from other cells in the network. We assume that it is of the form:

$$I_{syn_i} = g_{syn_i} \times s_i^{tot} \times (V_i - V_{syn}) \quad (5)$$

where, g_{syn} is the maximal synaptic conductance and V_{syn} is the synaptic reversal potential. If g_O , g_R and g_P represent the maximal synaptic conductances for O, R and P, respectively, then $g_{syn} \equiv g_O = g_P = 2g_R$. Further for each cell, s_i^{tot} is defined as:

$$s_i^{tot} = \begin{cases} s_R, & \text{if } i = O \text{ or } P \\ \frac{1}{2}(s_O + s_P), & \text{if } i = R \end{cases} \quad (6)$$

where s_O , s_R and s_P correspond to the influence of pre-synaptic potentials on the post-synaptic conductance; each of these satisfies the scalar equation (4). Hence, the synaptic currents are given by, $I_{syn_O} = g_O \times s_R \times (V_O - V_{syn})$, $I_{syn_R} = g_R \times (s_O + s_P) \times (V_R - V_{syn})$, $I_{syn_P} = g_P \times s_R \times (V_P - V_{syn})$ for O, R and P respectively. In equation (4), α and β_i correspond to the rate of

activation and rate of inactivation of the synapses, where α is the same for all the three cells in the network, whereas β_i may vary; $s_\infty(V_i)$ is the steady state synaptic activation function.

The nonlinear functions in the model are given by:

$$\begin{aligned}
 m_\infty(V_i) &= 0.5 \frac{1.0 + \tanh(V_i + 1.2)}{18} \\
 w_\infty(V_i) &= 0.5 \frac{1.0 + \tanh(V_i - 12)}{17.4} \\
 \tau(V_i) &= \frac{1}{\cosh(V_i - \frac{12}{34.8})} \\
 s_\infty(V_i) &= \frac{1}{1 + e^{-(V_i - \theta_s)/K_s}}
 \end{aligned}$$

The parameter values are given in Table 1 for the network behaviors described in the following section. Simulations were performed using the software XPPAUT (Ermentrout, 2002).

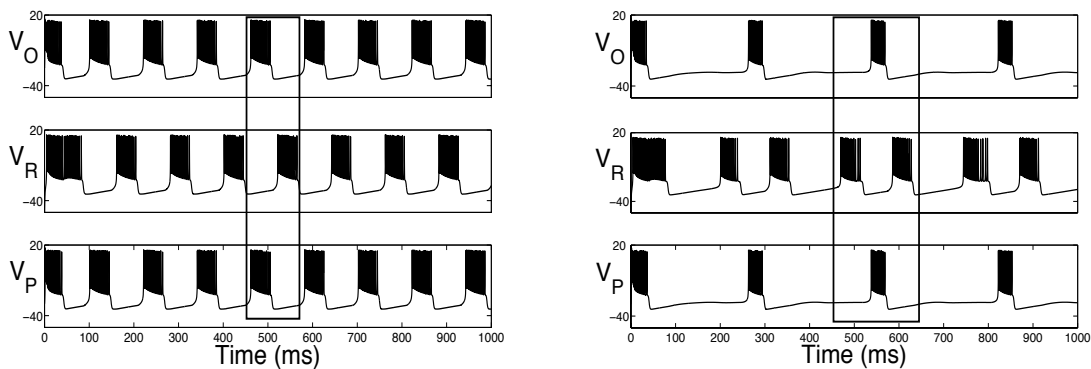
Parameter	Value	Parameter	Value
g_L	2.0 nS/ μm^2	θ_{syn}	-28.0 mV
g_{Ca}	4.0 nS/ μm^2	V_{syn}	-100 mV
g_K	8.0 nS/ μm^2	α	2.0
g_{KCa}	0.25 nS/ μm^2	β_O	0.03
V_{Ca}	120.0 mV	β_P	0.03
V_K	-84.0 mV	β_R	Lick \rightarrow 0.03, Gape \rightarrow 0.003
V_L	-60.0 mV	g_O	0.1 nS/ μm^2
ϕ	0.23	g_P	0.1 nS/ μm^2
ε	0.00125	g_R	0.05 nS/ μm^2
μ	0.01	I	50 μA

Table 1: Parameter Values

3 Numerical Results - Network Activity

Figure 4 demonstrates two different activity patterns similar to licks and gapes generated by the model. The membrane potentials of O, R and P during network activity similar

to licks are shown in Figure 4(a). A single lick cycle with a burst of synchronized activity in O and P (phase-I) followed by a burst of activity in R (phase-II) is highlighted in the figure. These lick cycles repeat at about 8 Hz comparable to EMG burst rate during licks. Figure 4(b) shows the membrane potentials of O, R and P during activity similar to gapes. This consists of repeating cycles of burst of activity in R (phase-I) followed by synchronized bursts of O and P (phase-II) terminating with additional burst of activity in R (phase-III) as highlighted in the figure. The gape cycles repeat at about 3Hz similar to experiments. Note that during each lick cycle, the cells burst precisely once. However, during each gape cycle, R bursts twice while O and P burst just once.



(a) Lick activity pattern in O, R and P generated by the model

(b) Gape activity pattern in O, R and P generated by the model

Figure 4: Membrane potentials (mV) during lick and gape network activity; Single lick and gape cycles are highlighted in (a) and (b) respectively

In order to switch from lick to gape pattern, we changed the parameter β_R , corresponding to the decay rate of inhibition from cell R to cells O and P. When $\beta_O = \beta_R = \beta_P = 0.03$, the lick pattern ensues with anti-phase behavior of O and P with R. When $\beta_O = \beta_P = 0.03$ and $\beta_R = 0.003$, the inhibition generated by R decays about 10 times slower than the inhibition generated by O and P; in this case, a pattern similar to gape results. In the following section we provide geometric analysis of the solutions in order to describe how

lick and gape behaviors can emerge by the appropriate choice for β_R .

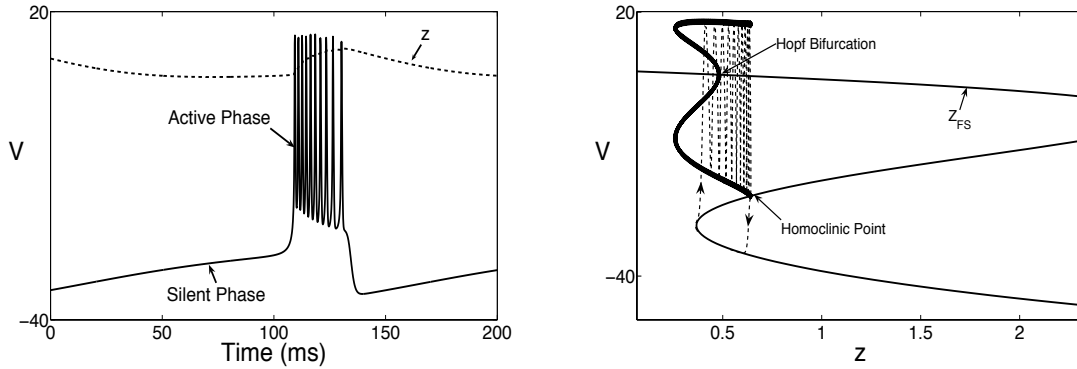
4 Geometric Analysis

4.1 Single Isolated Cell

We begin by considering a single cell without any coupling; that is, we consider equations (1)-(3) with $I_{syn_i} = 0$ for all 3 cells. A single cell exhibits square-wave bursting and geometric singular perturbation methods are very useful in understanding how bursting activity arises (Rubin & Terman, 2002).

The first step in the analysis is to dissect the system into fast and slow subsystems. Numerical simulations indicate that the calcium concentration Ca varies slowly in comparison with other dependent variables (V and w). Figure 5(a) shows the membrane potential during a single burst. In the figure the slow dynamics of the gating variable z that depends on near membrane Ca^{2+} concentration is also shown. The slow calcium dynamics is also evident from the fact that $\varepsilon > 0$ is small in equation (3). Hence, we treat equations (1) and (2) as the fast subsystem (FS) and equation (3) as the slow equation. If $\varepsilon = 0$, then Ca is constant and we can consider the gating variable z to be a bifurcation parameter in (FS). Figure 5(b) shows the corresponding bifurcation diagram of (FS). The Z-shaped curve Z_{FS} represents a curve of fixed points of (FS). The lower branch of Z_{FS} consists of stable fixed points of (FS), while the middle branch of Z_{FS} are saddles. The upper branch consists of both stable and unstable fixed points. A subcritical Hopf bifurcation occurs along the upper branch of Z_{FS} . This gives rise to a branch of unstable periodic solutions of (FS). This branch "turns around" to form a branch of stable limit cycles that terminates along a solution of (FS) that is homoclinic to one of the fixed points along the middle branch of Z_{FS} .

The projection of the bursting solution onto the bifurcation diagram is shown in Fig-



(a) Membrane potential during a single burst of activity in an isolated cell; Calcium gating variable z is superimposed to show the slow dynamics

(b) Bifurcation diagram of the fast subsystem (FS) with z as the bifurcation parameter. Z_{FS} is a Z-shaped curve of fixed points of (FS); Hopf bifurcation and homoclinic points are shown; the dashed line shows the bursting solution

Figure 5: Burst characteristics and bifurcation diagram for single isolated cell

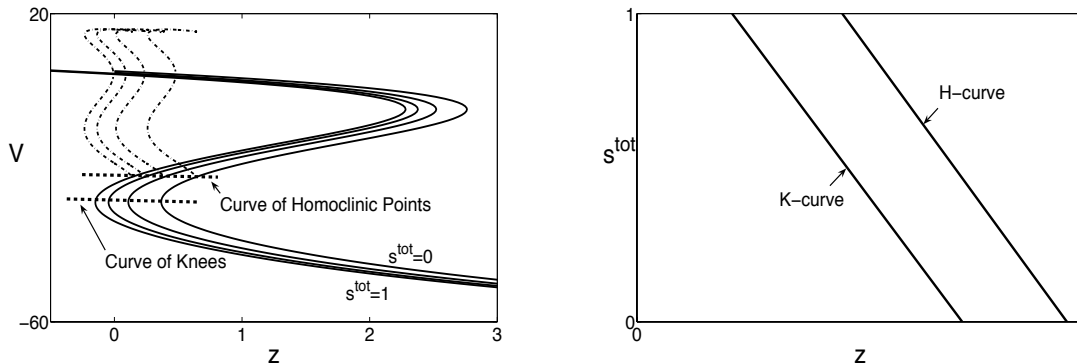
ure 5(b). When the membrane is not firing, the solution lies close to the lower branch of Z_{FS} , consisting of stable fixed points of (FS). During this resting state, intracellular Ca^{2+} concentration slowly decreases and hence z decreases. This causes the solution to drift towards the left knee of Z_{FS} . Upon reaching the left knee, the bursting solution jumps up to near the branch of stable limit cycles of (FS) and the active/firing phase begins. Note that the I_{Ca} now brings more Ca^{2+} into the cell and the variables Ca and z slowly increase. As z increases, the solution continues to spike until it reaches a neighborhood of homoclinic orbit of (FS). Once past the homoclinic orbit, the solution is forced back to the lower branch of Z_{FS} . This is equivalent to the slow accumulation of intracellular Ca^{2+} that eventually turns on the outward I_{KCa} current. When I_{KCa} is sufficiently large, the cell can no longer maintain its depolarized state. Hence, firing terminates and the cell returns to rest. This completes one cycle of the bursting solution.

4.2 Coupled Cells

In the presence of inhibitory coupling, the equations for each cell in the network are given by equations (1)-(4). We will analyze network activity using fast/slow analysis, similar to that in the preceding section. We will assume that $\beta = O(\varepsilon)$ so that s^{tot} decays on the slow time scale for each cell. Hence, there are now two slow variables corresponding to each cell, namely Ca and s^{tot} . As in the preceding section, equations (1) and (2) form the fast subsystem (FS) and we consider the bifurcation diagram of (FS). Unlike the preceding section, there are now two bifurcation parameters, that is, z and s^{tot} .

We first fix s^{tot} and compute the bifurcation diagram of (FS) with z as the bifurcation parameter. Figure 6(a) shows that for each value of s^{tot} , there is a Z-shaped curve of fixed points. The union of these curves forms a Z-shaped surface. Along this surface lies a curve of left knees and a curve of homoclinic points. The projections of these curves onto the (z, s^{tot}) slow phase plane are shown in Figure 6(b); we denote these projections as the K-curve and the H-curve, respectively. For values of (z, s^{tot}) that lie between the K- and H-curves, (FS) is bistable. That is, there is both a stable fixed point that lies along the lower branch of the Z-shaped surface and a stable limit cycle.

In the following sections, we will analyze the lick and gape patterns by considering the projections of solutions onto the (z, s^{tot}) slow phase plane. Since there are three cells, we need to follow three points as they evolve in this plane. In general, a cell's silent phase terminates once the point corresponding to that cell falls below the K-curve. The cell's active phase terminates when the point reaches the H-curve. We note that while the synaptic variables turn off on the slow time scale, they activate on the fast time scale. Hence, if a cell that is silent crosses the K-curve, then that cell will immediately start to spike and its synaptic variable will be reset to 1; the reset is instantaneous with respect to the slow time scale. This will then change the positions of the points corresponding to the other cells.



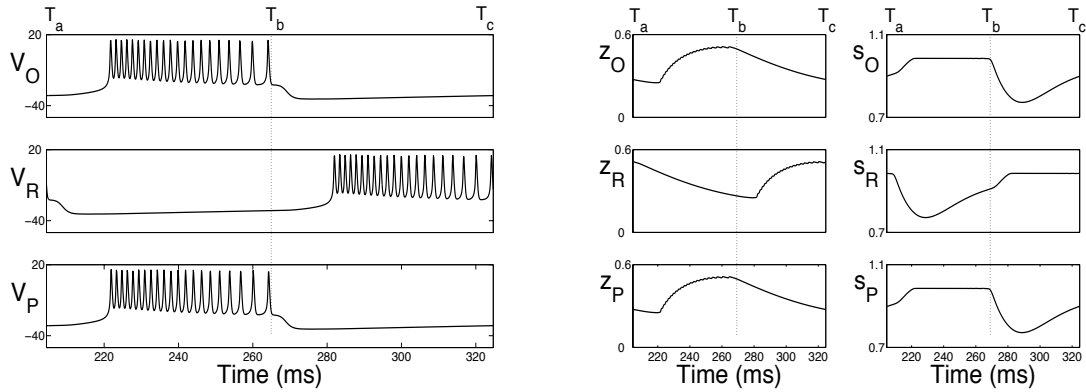
(a) Bifurcation curves with z and s as bifurcation parameters and resulting K-H curves

(b) Slow variable phase plane (z - s) showing the curve of left knee points (K-curve) and the curve of homoclinic points (H-curve)

Figure 6: Bifurcation curves for (FS)

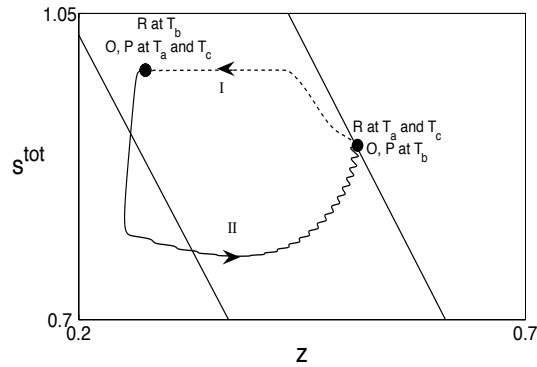
4.3 Geometric Analysis of the Lick Pattern

As described earlier, lick cycles are characterized by alternating phases of tongue protrusion with coincident jaw opening marked by activity in O and P (phase-I), and tongue retraction marked by activity in R (phase-II). We begin by considering a single lick cycle in the interval $[T_a, T_c]$. Figure 7(a) shows the membrane potentials ($V_{O,R,P}$) and Figure 7(b) shows time courses of the calcium-gating variables ($z_{O,R,P}$) and the synaptic variables ($s_{O,R,P}$) during $T_a \leq t \leq T_c$. In the interval $[T_a, T_b]$, O and P are co-active and R is silent and in the interval $[T_b, T_c]$, R becomes active and O and P return to silent phase. Note that a cell's calcium-gating variable decreases when the cell is silent and increases when the cell is active. The synaptic variable remains fully activated, i.e. $s \approx 1$, while the cell is active. The synaptic variable slowly decreases during most of the cell's silent phase; note that the synaptic variable slowly increases towards the end of the silent phase as the cell becomes more depolarized. As mentioned before s^{tot} is the synaptic input that each cell receives and is defined in equation (6). For O and P cells, we will trace (z_O, s_O^{tot}) and (z_P, s_P^{tot}) respectively and for R cell, we will trace (z_R, s_R^{tot}) in the (z, s^{tot}) phase-plane.



(a) Membrane potentials of O, R and P during licks in the interval $T_a \leq t \leq T_c$ marking a single lick cycle

(b) Time course of slow variables (z_O, z_R, z_P) and (s_O, s_R, s_P) during $T_a \leq t \leq T_c$



(c) Projection of points (z_O, s_O^{tot}) , (z_P, s_P^{tot}) and (z_R, s_R^{tot}) in the (z, s^{tot}) phase plane during the interval $T_a \leq t \leq T_c$

Figure 7: Analysis of lick cycle

Figure 7(c) shows the projection of the solution corresponding to each cell onto the (z, s^{tot}) phase-plane in the interval $T_a \leq t \leq T_c$. The position of each cell at time T_a is shown and the arrows indicate the direction of the trajectory. When $t = T_a$, R lies close to the H-curve; that is, R's trajectory crosses the homoclinic curve and its active phase terminates. At this time, both O and P are silent. The trajectory for each cell in the (z, s^{tot}) phase plane during $[T_a, T_b]$ is shown indicating phase-I of the lick cycle. Once R

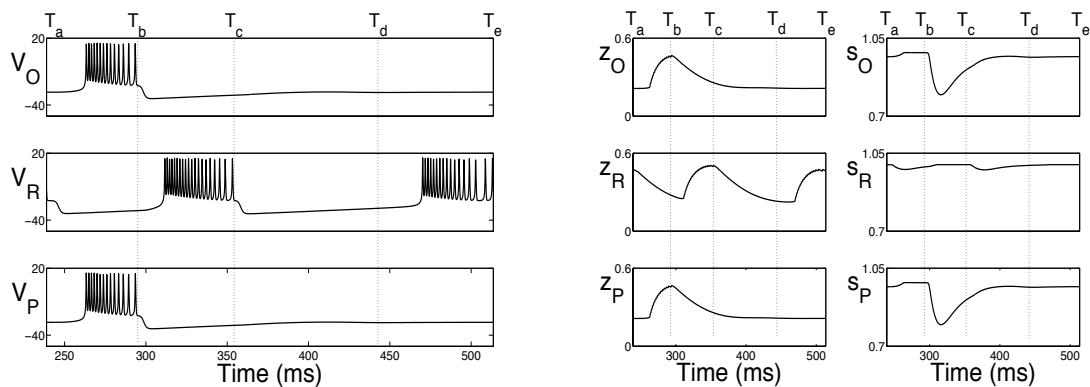
stops spiking, its synaptic variable s_R slowly decreases. Since $s_O^{tot} = s_P^{tot} = s_R$ for O and P, it follows that during this time, (z_O, s_O^{tot}) and (z_P, s_P^{tot}) move downwards for these two cells. Eventually, both of these points cross the K-curve, at which time O and P leave the silent phase. After a slight delay, O and P enter the active phase and begin to spike. At this time, both s_O and $s_P \rightarrow 1$ on the fast time scale. Hence, $s_R^{tot} = \frac{1}{2}(s_O + s_P) \rightarrow 1$ for R which now feels maximum inhibition and cannot fire. While O and P are active, their calcium-gating variables, z_O and z_P , increase and since R is silent, z_R decreases. At time T_b when (z_O, s_O^{tot}) and (z_P, s_P^{tot}) cross the H-curve, the active phases of O and P terminate.

The trajectory for each cell in the (z, s^{tot}) phase plane during $[T_b, T_c]$ shows that at time T_b when (z_O, s_O^{tot}) and (z_P, s_P^{tot}) cross the H-curve, O and P stop spiking and their synaptic variables s_O and s_P slowly decrease. Since $s_R^{tot} = \frac{1}{2}(s_O + s_P)$, it follows that (z_R, s_R^{tot}) for cell R moves downwards until it crosses the K-curve. At this time, R leaves the silent phase and, after a slight delay, begins to spike. Once this happens, $s_R \rightarrow 1$ and both O and P receive maximum inhibition. Since R is active, its calcium-gating variable z_R increases until (z_R, s_R^{tot}) reaches the H-curve and subsequently terminates firing. This completes one lick cycle.

4.4 Geometric Analysis of the Gape Pattern

A gape cycle consists of an initial burst of activity in R (phase-I) followed by synchronized bursts of O and P (phase-II) terminating with an additional burst of activity in R (phase-III). Note that we set the rate of decay of inhibition β_R on O and P to be 10 times slower than the rates of decay of inhibition (β_O and β_P) on R and the network pattern switches to gapes. We will select the interval $T_a \leq t \leq T_e$ to describe the evolution of trajectory in the (z, s^{tot}) geometric phase plane. Figure 8(a) shows the membrane potentials ($V_{O,R,P}$) and Figure 8(b) shows time courses of the calcium-gating variables ($z_{O,R,P}$) and the synaptic variables ($s_{O,R,P}$) in the interval $[T_a, T_e]$. We choose T_a such that at this time, R terminates

bursting activity marking the end of phase-I of a gape cycle. For $T_a \leq t \leq T_b$, cells O and P exhibit synchronized bursts and R is silent. During $T_b \leq t \leq T_c$, R is active, while O and P are silent. All of the cells are silent for $T_c \leq t \leq T_d$ and cell R exhibits another burst during $T_d \leq t \leq T_e$, while O and P are silent. As before, we will trace (z_O, s_O^{tot}) , (z_P, s_P^{tot}) and (z_R, s_R^{tot}) for O, P and R respectively in the (z, s^{tot}) phase plane. In what follows, we will step through each interval described above in order to describe the geometric mechanisms underlying this rhythm. This analysis will be very useful in understanding why changing β_R , the rate of decay of s_R , allows for the switch between lick and gape patterns.



(a) Membrane potentials of O, R and P for gape pattern in the interval $T_a \leq t \leq T_e$ defining the duration of solution used for geometric analysis

(b) Time course of slow variables (z_O, z_R, z_P) and (s_O, s_R, s_P) during $T_a \leq t \leq T_e$

Figure 8: Gape activity during $T_a \leq t \leq T_e$

When $t = T_a$, phase-I of the gape cycle (see Figure 8(a)) just ends marked by the termination of R firing. In Figure 9(a), the (z, s^{tot}) traces for O, P and R are shown for the interval $[T_a, T_b]$. At $t = T_a$, (z_R, s_R^{tot}) lies close to H-curve while (z_O, s_O^{tot}) and (z_P, s_P^{tot}) are close to the K-curve. After a certain delay, O and P enter the bursting phase. Note that $s_R^{tot} \rightarrow 1$ indicating that R now feels maximum inhibition. Further z_R is gradually decreasing and hence R remains silent.

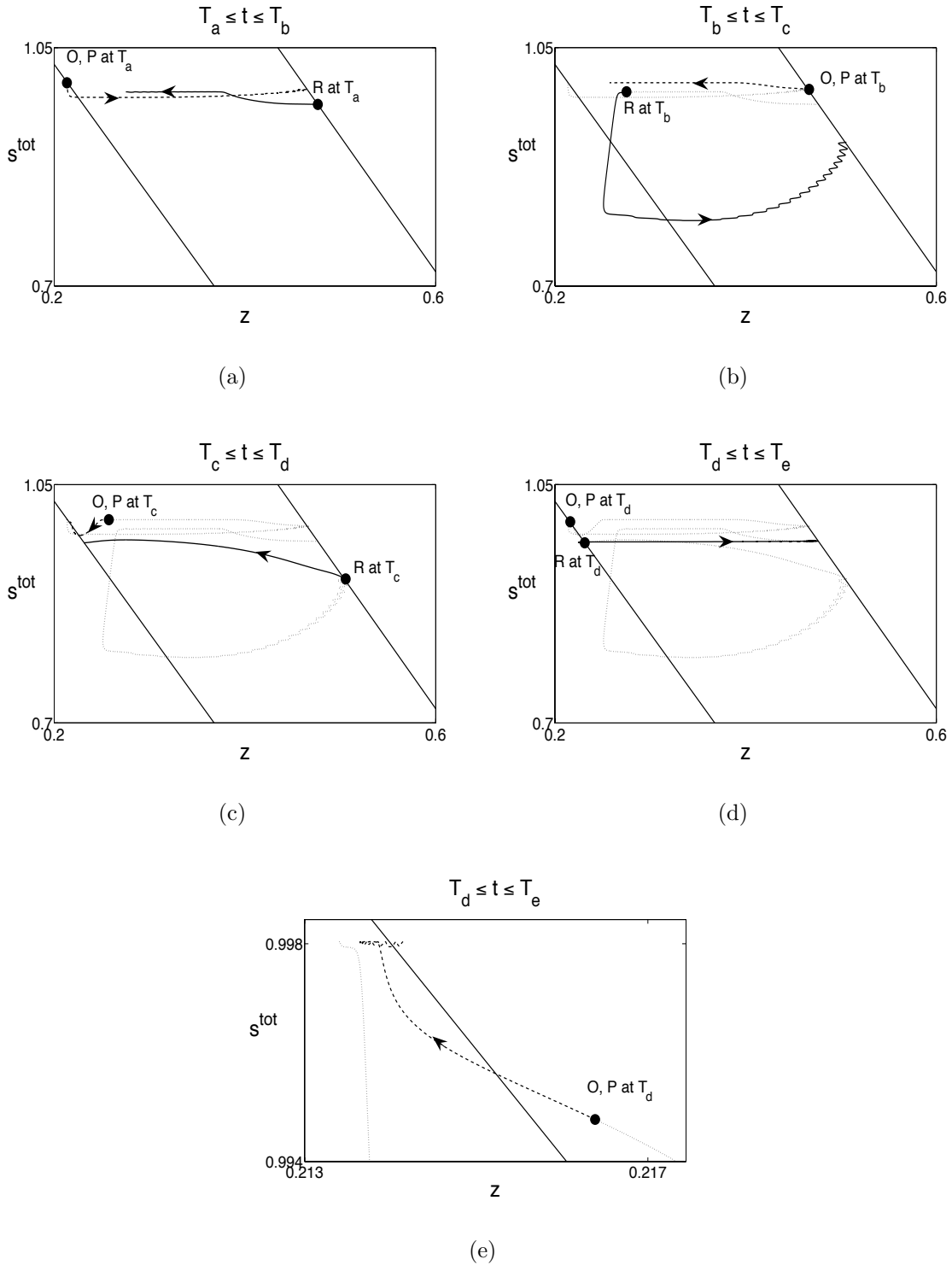


Figure 9: Geometric (z, s^{tot}) phase plane figures for gape activity during $T_a \leq t \leq T_e$. 9(a) - 9(e) Evolution of trajectory during the intervals shown in the figures; Relative positions of the cells at various time points are shown; Solid line represents the trace of (z_R, s_R^{tot}) , dashed line represents the traces of (z_O, s_O^{tot}) and (z_P, s_P^{tot}) in the current interval; dotted lines represent the trajectory in the previous intervals considered

When $t = T_b$, both (z_O, s_O^{tot}) and (z_P, s_P^{tot}) lie along the H-curve, signaling the termination of their bursting activity. These cells remain silent for $T_b \leq t \leq T_c$ (see Figure 9(b)), during which time their synaptic variables s_O and s_P decay at the rate $\beta_O = \beta_P$. Hence, for cell R, (z_R, s_R^{tot}) moves vertically downwards until it falls below the K-curve at time T_b . This corresponds to when R leaves the silent phase and, after a slight delay, begins a bursting episode. Cell R remains active for $T_b \leq t \leq T_c$. During this time, $s_R \rightarrow 1$ so that O and P receive maximum inhibition and remain in their silent phases as shown in Figure 9(b). Moreover, z_R increases while z_O and z_P decrease. This continues until (z_R, s_R^{tot}) reaches the H-curve at $t = T_c$, indicating the termination of R's active phase.

All the cells are silent for $T_c \leq t \leq T_d$ as noted in Figure 9(c). All of the calcium-gating variables decay during this time so that each of the points (z_O, s_O^{tot}) , (z_P, s_P^{tot}) and (z_R, s_R^{tot}) move towards the K-curve. There is now, in some sense, a race to see which of these points reaches the K-curve first. This will be the cell that is able to escape the silent phase and initiate the next phase of bursting activity. Note that when $t = T_c$, the points (z_O, s_O^{tot}) and (z_P, s_P^{tot}) are closer to the K-curve than (z_R, s_R^{tot}) which, at that time, lies along the H-curve. However, the points (z_O, s_O^{tot}) and (z_P, s_P^{tot}) evolve approximately ten times slower than (z_R, s_R^{tot}) . This is because β_R is set to be ten times smaller than β_O and β_P . For this reason, (z_R, s_R^{tot}) is, in fact, able to reach the K-curve first and R is the next cell to initiate an active phase. We assume that this occurs when $t = T_d$.

At T_d , cell R reaches the K-curve. After a slight delay, R jumps up to the active phase and remains active until T_e . During this time, cells O and P lie in the silent phase. Note in Figure 9(e) that both of these cells actually cross the K-curve, so one may have expected that they should jump-up to the active phase. However, we note that the K-curve predicts the jump-up points when the singular perturbation parameter ϵ has been formally set equal to zero. Since ϵ is small but not zero in our computations, it is possible for a cell to lie just below the K-curve and remain silent. This is, in fact, what happens here. The

cells O and P remain silent until $t = T_e$ when (z_R, s_R^{tot}) reaches the H-curve, signaling the termination of R's active phase.

The steps described for $[T_a, T_e]$ repeat leading to repetitive gape cycles. The existence of the gape pattern depends crucially on having β_R sufficiently smaller than β_O and β_P . This allows for (z_R, s_R^{tot}) to reach the K-curve and escape the silent phase at $t = T_d$, thus allowing R to fire two bursting episodes in a row. This fact that β_R is sufficiently smaller than β_O and β_P slows down the rate of recovery from inhibition and prolonging the hyperpolarization of O and P cells even after R cell stops firing enabling network activity to switch to gapes. We note that R does not fire more than two bursts in a row because (z_O, s_O^{tot}) and (z_P, s_P^{tot}) are closer to the H-curve after the second R-burst at $t = T_e$ than they were after the first R-burst at $t = T_c$. This is because z_O and z_P keep decreasing as long as O and P are silent for $T_b \leq t \leq T_e$, getting these two points closer to the K-curve during this time. If we choose β_R to be even smaller, then it is possible for R to fire more than two consecutive bursts while the other cells are silent.

5 Discussion

We have developed a biophysical model for a CPG network driving licking (ingestion) and gaping (oral rejection) oromotor behaviors. The model demonstrates how one configuration of connections is sufficient to generate two different patterns of network activity similar to licks and gapes. Hence, it supports the hypothesis that a CPG with 3 classes of interneurons and minimal connections can produce lick and gape-like rhythmic activity patterns. The model reproduces the phase sequence and rate of activity of licks and gapes derived from EMG studies and predicts conditions under which a lick pattern can switch to a gape pattern. Although this model predicts one possible synaptic mechanism for pattern switching that could play a role in vivo, it does not incorporate mechanisms to explain

how certain aspects of lick and gape EMG responses, such as the duration and amplitude of individual bursts of activity change during licks and gapes, suggesting additional levels of neural complexity.

5.1 Organization of CPG for Mastication and Licking

Our dynamical model for licking/gaping differs from previous neural models of oral consummatory ingestive behavior. Previous mammalian models for feeding behaviors are connectional and have focused exclusively on mastication, i.e. rhythmic alternations of jaw-opener and jaw-closure muscles, and not specifically considered coordination with the tongue (Chandler & Tal, 1986; Nakamura & Katakura, 1995; Lund *et al.*, 1998). Although licking is not as complex a behavior as mastication (Thexton, 1992), both behaviors share a common functional morphology involving rhythmic coordination of the tongue and jaws and likely share a central nervous system substrate as well (reviewed in (Travers *et al.*, 1997)). In addition, previous block diagram models of mastication have assumed that a masticatory CPG is anatomically organized into two neuronal groups: one for generation of the masticatory rhythm, i.e. the basic rate of the rhythmic activity, and the other for the generation of the pattern of activities of the jaw, tongue and facial muscles (Nakamura & Katakura, 1995). Evidence for this distinction is not definitive, and there are studies to suggest both independence and interdependence of different motor parameters of CPG activity including cycle rate (frequency) of the movement, amplitude of EMG response, duration of EMG burst during a cycle and phase sequencing of activity in different muscles during a cycle (Lund *et al.*, 1984; Chandler & Tal, 1986; Chen *et al.*, 2001; Chen & Travers, 2003). Our assumption that the same neurons are involved with both rate and pattern derive from a behavioral pharmacological study in which a non-NMDA receptor antagonist was infused into the medullary RF (Chen & Travers, 2003). Both licking and gaping were suppressed, supporting the contention that both behaviors are organized within the

same RF region, but importantly, as behavior recovered from complete suppression, the rate of oro-rhythmic activity increased in parallel with a decrease in burst duration to normal (pre-drug) levels, i.e. the two EMG parameters changed together. This is not to say that inputs to the CPG from other sources cannot influence rate or pattern independently (Chandler & Tal, 1986; Scott *et al.*, 1998), but does affirm that both empirically and theoretically, one common set of neurons can control rate and pattern.

5.2 Neurobiological Assumptions

In addition to the issues discussed above, our model assumes (1) three classes of interneurons, (2) neuronal bursting behavior, and (3) reciprocal inhibition. The existence of three (relatively) distinct classes of pre-oral motor neurons is well established (Travers & Norgren, 1983) and there are but few final common path interneurons with connections to more than one oral motor nucleus (Amri *et al.*, 1990; Popratiloff *et al.*, 2001; Li *et al.*, 1993). However, our model further assumes non-overlapping projections from pre-motor neurons to hypoglossal motor pool antagonists. Here, the anatomical data is sparse, but available evidence suggests that there is likely only a small population of pre-hypoglossal neurons that innervate both protruder and retractor motor pools (Travers & Rinaman, 2002). Such interneurons were not part of the proposed model and may play a role in lingual movements where co-activation of muscle antagonists is more pronounced than licking, for example respiratory gasping (Fuller *et al.*, 1998). However, gaping responses too have a component of co-activation of protruder and retractor muscles that could involve recruitment of such pre-motor interneurons (Travers *et al.*, 2000). Although there is a clear double contraction of lingual retractor muscles (styloglossus) during a gape that differentiates it from a lick cycle, the initial activation of the styloglossus is often accompanied by a lesser activation of tongue protruders that builds to a maximum response as the styloglossus becomes inactivated. This "nuance" of the gape response was not emer-

gent from our model and could involve other neural mechanisms not incorporated into the present model, for example recruitment (Dinardo & Travers, 1994; DiNardo & Travers, 1997).

Less is known of the bursting properties of pre-omomotor interneurons, but it is clear that many RF interneurons are rhythmically active during both fictive (Inoue *et al.*, 1994) and natural (Travers *et al.*, 2000) licking and chewing. Although putative pre-omomotor neurons in the RF appear highly heterogeneous in nature (Travers *et al.*, 2000), extracellular recording suggests that some of the lick-rhythmic RF neurons have a well characterized burst structure similar to square wave bursters (Rinzel, 1985), thus providing the initial basis for selecting the biophysical properties of the individual cells in the network. However, extracellular recording does not provide a biophysical description of the bursting characteristics of these neurons and, thus requires further study. Our logic in restricting the model to this one category of bursting neurons was to provide a "minimal" model that accounts for as much behavior as possible and to anticipate adding additional complexity (for example, additional neuron types), as we empirically validate or invalidate components of the model.

Lastly, we assumed a specific pattern of reciprocal inhibition between the 3 classes of interneurons. This is, perhaps, the most speculative of our assumptions but not one without some empirical support (Nakamura & Katakura, 1995; Travers *et al.*, 1997). In the context of locomotion (Buchanan, 1982a,b) and mastication (Inoue *et al.*, 1994), there is evidence of phasic inhibition mediated by glycine receptors between CPG interneurons driving functionally antagonist muscles. Further, from EMG data, we note that GEN (tongue protruder) and STY (tongue retractor) activity show functional antagonism during licks and gapes. Hence the connection between the pre-motor neurons driving these muscles (R and P) has been modeled as reciprocal inhibition. The determination of the precise patterns of reciprocal inhibition assumed by our model awaits further empirical

work.

With these basic neurobiological assumptions, parameter values such as synaptic conductances were suitably chosen to obtain the expected network behavior. Typical values were used for reversal potentials and maximal conductance for specific ionic currents (see Table 1). Gating functions and variables were chosen to describe the non-linear characteristics of ion channels. Pattern switching occurs due to change in the rate of decay (β_R) of the inhibitory synaptic input from R to O and P cells. When the rate of onset and decay of the synaptic variables (s_O , s_R and s_P) are identical, an antiphase-behavior consisting of phase-I (O and P active and R silent) and phase-II (O and P silent and R active) produces results similar to licks. When the rate of decay of s_O^{tot} and s_P^{tot} is made about 10 times slower (by changing β_R from 0.03 to 0.003), the network pattern switches to gapes. This dynamic behavior that crucially depends on the evolution of slow variables ($s_{O,R,P}$) has been explained using geometric phase-plane analysis and fast-slow reduction of the system of equations. Hence, the model predicts that modulation of the time-scale of inhibitory synaptic conductance could be a possible mechanism leading to pattern switching from licks to gapes.

5.3 Role of Inhibition in Pattern Switching

Several empirical examples show how the time-scale of inhibition can be modulated directly by different durations and rates of onset and decay of inhibitory postsynaptic currents (via ionotropic mechanisms), or indirectly by altering intrinsic conductances (via metabotropic mechanisms). In our model, the network changes from a pattern of licks to gapes when there is about a 10-fold decrease in the rate of decay of s_O^{tot} and s_P^{tot} which leads to prolonged inhibition of O and P cells. This prevents faster recovery from inhibition in these cells and decreases their burst rate from ≈ 8 Hz (licks) to ≈ 4 Hz (gapes). Studies on lamprey locomotion demonstrate how burst rate decreases due to prolonged hyperpolar-

ization. The activation of metabotropic GABA_B receptors on lamprey spinal cord CPG interneurons depresses a low-threshold transient inward calcium current I_T , which leads to a longer hyperpolarized phase and a delayed spike onset (Matsushima *et al.*, 1993; Tegner *et al.*, 1993). As a result, the interneurons show slow recovery from inhibition and a consequent slowing in the overall (swimming) rate. Within this network, the conductance changes for a specific intrinsic current (I_T) on both sets of antagonist interneurons. In our model, we posit a change in an unidentified hyperpolarizing synaptic conductance that influences only specific interneurons to produce a switch in network activity from licks to gapes. Validation of this assumption awaits future experiments to determine specific intrinsic conductances as well as the existence of GABA_B receptors on lick-gape CPG interneurons.

Although numerous mechanisms exist to explain prolonged hyperpolarization, the approximately 10-fold decrease in the rate of decay of hyperpolarization in our model corresponds well to the decay rates of inhibitory post-synaptic currents due to activation of glycine and GABA_A receptors observed in hypoglossal and abducens motoneurons. Glycine and GABA_A receptors present on the same motoneuron have different time scales for the onset and decay of their inhibitory postsynaptic currents (O'Brien & Berger, 1999; Donato & Nistri, 2000; Russier *et al.*, 2002). Whole cell recording from these motoneurons in a slice preparation demonstrated that the distribution of decay times for glycine receptors peaked somewhere around 3-5 ms, compared to GABA_A receptors that peaked somewhere around 30 - 55 ms. Thus, a glycine receptor-mediated response which has fast onset and decay dynamics could ensure an immediate blockade of motoneuron firing whereas a GABA_A receptor-mediated response, which has slower onset and decay dynamics and hence longer duration could produce prolonged inhibition.

In the lick-gape circuit, we have previously demonstrated a role for GABA and glycine (Chen *et al.*, 2001; Chen & Travers, 2003). One could thus posit a mechanism where some

interneurons (O and P) have receptor for both glycine and GABA_A. If stimulation by the bitter taste, quinine monohydrochloride (QHCl), resulted in the release of GABA and activation of these GABA_A receptors with similar kinetics as the brainstem motorneurons, the sustained hyperpolarization could produce the rate and phase changes associated with gapes. Indeed, several lines of evidence suggest that QHCl activates a rather specific population of neurons in the nucleus of the solitary tract (Travers, 2002). Some of the output neurons appear to be GABA-ergic and have direct and/or indirect projections to the RF (Travers & Hu, 2000). Additional study, however will be required to demonstrate whether activation of GABA_A receptors due to QHCl stimulation can produce prolonged hyperpolarization as specified by the model. Because behavioral pharmacology studies "flood" the entire substrate with a ligand, more precise studies of receptor kinetics in identified neurons will be necessary to substantiate these predictions.

Acknowledgements

This work was partially funded by NIH grant DC00417 (JBT) and NSF grant DMS0514356 (DT). This work was also partially funded by NSF grant under agreement number 0112050. We thank Praveen Shankar for helpful comments and technical assistance.

References

- Amri M, Car A & Roman C (1990). Axonal branching of medullary swallowing neurons projecting on the trigeminal and hypoglossal motor nuclei: demonstration by electrophysiological and fluorescent double labeling techniques. *Exp Brain Res* 81: 384–90
- Buchanan JT (1982a). Activities of identified interneurons, motoneurons, and muscle fibers during fictive swimming in the lamprey and effects of reticulospinal and dorsal cell stimulation. *J Neurophysiol* 47: 948–60

- Buchanan JT (1982b). Identification of interneurons with contralateral, caudal axons in the lamprey spinal cord: synaptic interactions and morphology. *J Neurophysiol* 47: 961–75
- Chandler SH & Tal M (1986). The effects of brain stem transections on the neuronal networks responsible for rhythmical jaw muscle activity in the guinea pig. *J Neurosci* 6: 1831–42
- Chen Z & Travers JB (2003). Inactivation of amino acid receptors in medullary reticular formation modulates and suppresses ingestion and rejection responses in the awake rat. *Am J Physiol Regul Integr Comp Physiol* 285: R68–83
- Chen Z, Travers SP & Travers JB (2001). Muscimol infusions in the brain stem reticular formation reversibly block ingestion in the awake rat. *Am J Physiol Regul Integr Comp Physiol* 280: R1085–94.
- Dinardo LA & Travers JB (1994). Hypoglossal neural activity during ingestion and rejection in the awake rat. *J Neurophysiol* 72: 1181–91
- DiNardo LA & Travers JB (1997). Distribution of fos-like immunoreactivity in the medullary reticular formation of the rat after gustatory elicited ingestion and rejection behaviors. *J Neurosci* 17: 3826–39
- Donato R & Nistri A (2000). Relative contribution by GABA or glycine to Cl^- -mediated synaptic transmission on rat hypoglossal motoneurons in vitro. *J Neurophysiol* 84: 2715–24
- Ermentrout GB (2002). *Simulating, analyzing and animating dynamical systems*. SIAM Press: Philadelphia 2nd edn.
- Fuller D, Mateika JH & Fregosi RF (1998). Co-activation of tongue protruder and retractor muscles during chemoreceptor stimulation in the rat. *J Physiol* 507 (Pt 1): 265–76

- Grill HJ & Kaplan JM (2002). The neuroanatomical axis for control of energy balance. *Front Neuroendocrinol* 23: 2–40
- Grill HJ & Norgren R (1978). Chronically decerebrate rats demonstrate satiation but not bait shyness. *Science* 201: 267–9
- Hodgkin AL & Huxley AF (1952). A quantitative description of membrane current and its application to conduction and excitation in nerve. *J Physiol* 117: 500–44
- Inoue T, Chandler SH & Goldberg LJ (1994). Neuropharmacological mechanisms underlying rhythmical discharge in trigeminal interneurons during fictive mastication. *J Neurophysiol* 71: 2061–73
- Kupfermann I (1974). Dissociation of the appetitive and consummatory phases of feeding behavior in aplysia: a lesion study. *Behav Biol* 10: 89–97
- Li YQ, Takada M & Mizuno N (1993). Premotor neurons projecting simultaneously to two orofacial motor nuclei by sending their branched axons. a study with a fluorescent retrograde double-labeling technique in the rat. *Neurosci Lett* 152: 29–32
- Lund JP, Sasamoto K, Murakami T & Olsson KA (1984). Analysis of rhythmical jaw movements produced by electrical stimulation of motor-sensory cortex of rabbits. *J Neurophysiol* 52: 1014–29
- Lund JP, Kolta A, Westberg KG & Scott G (1998). Brainstem mechanisms underlying feeding behaviors. *Curr Opin Neurobiol* 8: 718–24
- Marder E & Pearson KG (1998). Editorial overview: motor control from molecules to bedside. *Curr Opin Neurobiol* 8: 693–6
- Matsushima T, Tegner J, Hill RH & Grillner S (1993). GABA_B receptor activation causes

- a depression of low- and high-voltage-activated Ca^{2+} currents, postinhibitory rebound, and postspike afterhyperpolarization in lamprey neurons. *J Neurophysiol* 70: 2606–19
- Nakamura Y & Katakura N (1995). Generation of masticatory rhythm in the brainstem. *Neurosci Res* 23: 1–19
- O'Brien JA & Berger AJ (1999). Cotransmission of GABA and glycine to brain stem motoneurons. *J Neurophysiol* 82: 1638–41
- Popratiloff AS, Streppel M, Gruart A, Guntinas-Lichius O, Angelov DN, Stennert E, Delgado-Garcia JM & Neiss WF (2001). Hypoglossal and reticular interneurons involved in oro-facial coordination in the rat. *J Comp Neurol* 433: 364–79
- Rinzel J (1985). *Bursting oscillations in an excitable membrane model, Ordinary and Partial Differential Equations*. Springer: New York
- Rinzel J & Ermentrout GB (1998). *Analysis of neural excitability and oscillations, Methods in neuronal modeling: from ions to networks*. Koch C and Segev I, MIT Press: Cambridge, MA 2nd edn.
- Rubin JE & Terman D (2002). *Geometric singular perturbation analysis of neuronal dynamics*. Fiedler B, Elsevier Science B. V. 2nd edn.
- Russier M, Kopysova IL, Ankri N, Ferrand N & Debanne D (2002). GABA and glycine co-release optimizes functional inhibition in rat brainstem motoneurons in vitro. *J Physiol* 541: 123–37
- Scott G, Westberg KG, Kolta A, Vrentzos N & Lund JP (1998). Organization of the brainstem pattern generator of mastication. *J Dent Res* 77–115
- Steiner JE (1973). The gustofacial response: observation on normal and anencephalic newborn infants. *Symp Oral Sens Percept* 4: 254–78

- Tegner J, Matsushima T, el Manira A & Grillner S (1993). The spinal GABA system modulates burst frequency and intersegmental coordination in the lamprey: differential effects of GABA_A and GABA_B receptors. *J Neurophysiol* 69: 647–57
- Thexton AJ (1992). Mastication and swallowing: an overview. *Br Dent J* 173: 197–206
- Travers JB & Norgren R (1983). Afferent projections to the oral motor nuclei in the rat. *J Comp Neurol* 220: 280–98
- Travers JB & Norgren R (1986). Electromyographic analysis of the ingestion and rejection of sapid stimuli in the rat. *Behav Neurosci* 100: 544–55
- Travers JB & Rinaman L (2002). Identification of lingual motor control circuits using two strains of pseudorabies virus. *Neuroscience* 115: 1139–51
- Travers JB, DiNardo LA & Karimnamazi H (1997). Motor and premotor mechanisms of licking. *Neurosci Biobehav Rev* 21: 631–647
- Travers JB, DiNardo LA & Karimnamazi H (2000). Medullary reticular formation activity during ingestion and rejection in the awake rat. *Exp Brain Res* 130: 78–92
- Travers SP (2002). Quinine and citric acid elicit distinctive fos-like immunoreactivity in the rat nucleus of the solitary tract. *Am J Physiol Regul Integr Comp Physiol* 282: R1798–810
- Travers SP & Hu H (2000). Extranuclear projections of rnsst neurons expressing gustatory-elicited fos. *J Comp Neurol* 427: 124–38